13th International Conference on
Structural Health Monitoring of Intelligent Infrastructure
DOI: 10.3217/978-3-99161-057-1-165

Utilizing PSDefoPAT® to analyze surface deformation of embankment dams

M. Evers[1, 2] A. Thiele [1,2]
[1]Fraunhofer IOSB, Gutleuthausstraße 1, 76275 Ettlingen, Germany
[2]Karlsruhe Institute of Technology, Kaiserstraße 12, 76131 Karlsruhe, Germany
email: madeline.evers@iosb.fraunhofer.de, antje.thiele@iosb.fraunhofer.de

ABSTRACT: Dams are used worldwide to, e.g., manage flooding, generate energy, or secure the freshwater supply. They play an essential role in the local economy. However, an operational or structural failure also poses a significant threat to the environment and the local economy. Therefore, it is vital to ensure their structural health and functionality.
In this study, we present the ground surface deformation of the Parapeiros-Peiros Dam during the later stages of its construction, first filling, and shortly afterwards. Since data services, such as the European Ground Motion Service, surfaced and provide freely available ground motion datasets, one might think that in-house processing of SAR data for surface deformation monitoring of critical infrastructure is obsolete. In order to explore the advantages of in-house processing, we compare ground motion datasets generated by Fraunhofer IOSB and the European Ground Motion Service based on advanced differential synthetic aperture radar interferometry techniques. The dataset consists of sets of measuring points, their mean deformation velocity, and the associated displacement time series. Based on the mean velocity maps, we present a spatial analysis of the observed deformation patterns. In addition, we analyzed the temporal deformation pattern of individual measuring points by employing the Persistent Scatterer Deformation Pattern Analysis Tool (PSDefoPAT®). This tool can be used to fully automatically identify the statistically best fitting model to describe the temporal deformation pattern of a persistent or distributed scatterer (i.e., linear, quadratic, piecewise linear, or periodic) and provides insight into the dynamics of the surface deformation. It can aid with the analysis of changes in the structural health of the dam.

KEYWORDS: Embankment Dam; Persistent Scatterer Interferometry; European Ground Motion Service; Deformation PSDefoPAT®.

1 INTRODUCTION

Dams are large engineering structures used for centuries to stop the surface water flow. They have at least two components: a dam body and a reservoir. The dam body is used to either redirect or impound surface water. The impounded water creates an artificial lake, which is referred to as a reservoir. The main purposes of these structures are storing water for irrigation or human consumption, energy generation, flood control, fish farming, and storing tailings. Thus, they have a significant influence on the local economy. They can have a positive impact on the region, but a failure of the dam body or an operational failure can also be detrimental to the local economy, human settlements, and the environment. Therefore, it is essential to ensure their structural health and functionality [1]. Depending on the construction type of the dam body, the set of parameters that need to be monitored varies. In the case of an embankment dam, which is the most common type used worldwide, the International Commission on Large Dams (ICOLD) stipulates monitoring structural deformations, movements, and temperature of the dam body, as well as uplift pressure, seepage, drainage rates and the chemical composition of the seepage water [2,3].

This study will focus on the surface deformation of embankment dams. Those dams are subject to numerous loads during their lifetime, which can result in the deformation or displacement of the entire or parts of the dam body [4]. Recent studies have demonstrated that Synthetic Aperture Radar Interferometry (InSAR) techniques, such as Persistent Scatterer Interferometry (PSI), can be used to map and analyze the surface deformation of dams for short phases of their lifetime [5,6].

In this study, we map and analyze the deformation of the Parapeiros-Peiros dam during the time of the first filling of its reservoir and shortly after. The dam is located in southern Greece on the Peloponnese Peninsula. Its construction finished in early 2019, and the reservoir filling process started in September 2019. We acquired two different datasets of the area of interest. The first dataset, Dataset A, consists of 119 Sentinel-1 (S1) Synthetic Aperture Radar (SAR) images and was processed in-house. The second dataset, Dataset B, was obtained from the European Ground Motion Service (EGMS), which provides ground surface deformation measurements for most European countries based on S1 SAR images and advanced DInSAR processing. Dataset B covers the time from January 2019 to December 2023. Since data services, such as the EGMS, are freely available, one might think that in-house processing of SAR data for surface deformation monitoring of critical infrastructure is obsolete. However, the EGMS does not provide customized datasets for specific events or time spans and is delayed by at least three quarters of a year. In order to explore the advantages of in-house processing, we compare our own results with those generated by the EGMS regarding the observable spatial and temporal deformation patterns. Both datasets provide maps with the mean deformation velocities and displacement time series for individual measuring points (MP). The mean deformation velocity maps were used to

DOI: 10.3217/978-3-99161-057-1-165

analyze the spatial deformation pattern of the Parapeiros-Peiros dam, while the individual displacement time series were analyzed using the Persistent Scatterer Deformation Pattern Analysis Tool (PSDefoPAT®) developed at Fraunhofer IOSB, which automatically assigns each time series a best-fitting model [7]. The estimated time series models offer information on the temporal deformation pattern, which is not directly visible in the mean deformation velocity maps.

This paper is structured into five sections. The Parapeiros-Peiros dam and the data used to monitor it are described in Section 2. Section 3 provides an overview of the methods used to analyze the data. The results are presented and discussed in Section 4, and finally, our conclusion is presented in Section 5.

2 PARAPEIROS-PEIROS DAM

The Parapeiros-Peiros dam is located in the municipality of Patras in the northwest of the Peloponnese Peninsula (Greece). It consists of an embankment dam, a diversion dam, and a reservoir. The total capacity of its reservoir is 44 million m³ of water. The impounded water is intended to supply more than 2 million people in three regions (Patras, Erymanthos, and Dytiki Achaia) with fresh water. While the diversion dam reroutes the Peiros River, the embankment dam impounds the water of the Peiros and Parapeiros rivers. In detail, the dam is about 75 m high and 900 m long. Its construction finished in early 2019, and the filling process of the reservoir started in September 2019 [8,9] and. is estimated to take about three years.

The first reservoir filling is particularly interesting, since the construction is subject to all the loads it was built to withstand for the first time. The dam body is expected to deform as a consequence. At this point, only the most significant deformation phenomena will be mentioned. A detailed description of the many deformation phenomena was provided by Evers [10]. The deformation phenomena can be sorted into three patterns:

(1) subsidence,
(2) uplift and
(3) horizontal displacement.

The building and foundation materials of the dam body are compressed by the weight of the construction, resulting in partial or complete subsidence of the dam body. The dead load of the increasing amount of impounded water only fosters this process [11]. Moreover, collapse compression on the upstream shoulder can add to the subsidence rates. A partial uplift of the dam body can be caused by a decrease in the effective stress in the upstream shoulder resulting from the increasing water load during the filling process. The third deformation category is the horizontal displacement of the entire or parts of the dam body. The cause for horizontal displacement is the increased lateral tension within the dam body during the filling process [4].

Two advanced DInSAR datasets were used to analyze the spatial and temporal deformation of the Parapeiros-Peiros dam. The goal is to explore whether it is obsolete to process SAR images in-house for surface deformation monitoring of critical infrastructure such as dams, since ground motion datasets are freely available and updated regularly.

Dataset A consists of 119 S1 SAR images recorded with a descending acquisition geometry and Interferometric Wide Swath mode. The time series extends from September 2019 to November 2022, which corresponds to the time of the first filling of the reservoir. The images depict the area surrounding the Parapeiros-Peiros dam, allowing for the mapping and analysis of the deformation of the dam body and the surrounding slopes. Dataset B is a ground motion dataset of the same area provided by the EGMS. The EGMS provides ground motion measurements at a millimeter scale using persistent scatterer (PS) and distributed scatterer (DS) techniques. The service was first made available at the beginning of 2022 and documented in its first edition the ground motion of most European countries from 2015 to 2020 based on all available S1 images from this time span. The dataset is regularly updated, always considering S1 images of the past five years [12]. The new dataset is made available in the following fall. For this study, a dataset covering the period from January 2019 to December 2023 was used, which corresponds to the time immediately preceding the first filling, the first filling itself, and approximately two years afterward. The chronology of the datasets and the time of the construction and commission phase of the Parapeiros-Peiros dam they cover are illustrated in Figure 1. The goal is to explore whether

3 METHODS

3.1 Persistent Scatterer Interferometry (PSI)

InSAR and PSI are techniques used to map surface deformation

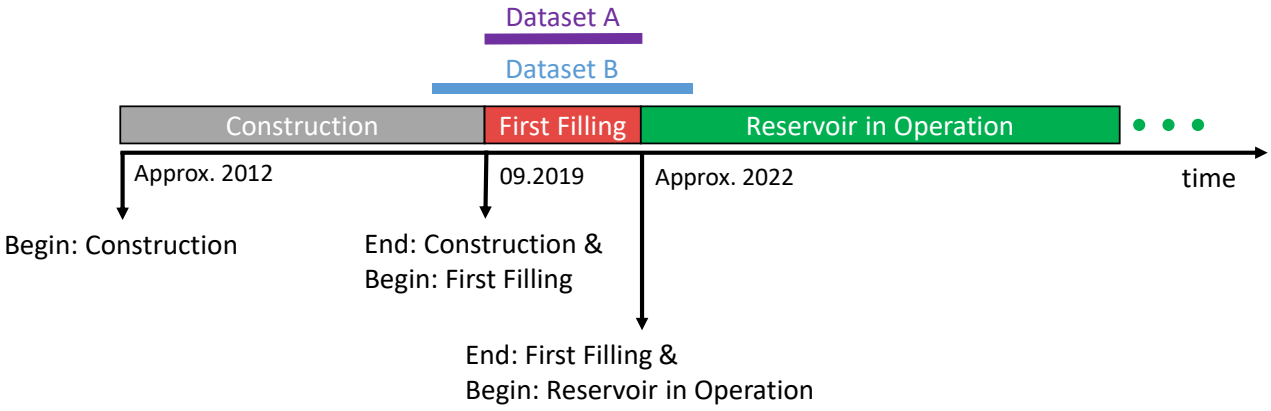

Figure 1. Timeline of the construction and commission phase of the Parapeiros-Peiros dam and the Datasets A (S1 images processed by Fraunhofer IOSB) and B (provided by EGMS).

DOI: 10.3217/978-3-99161-057-1-165

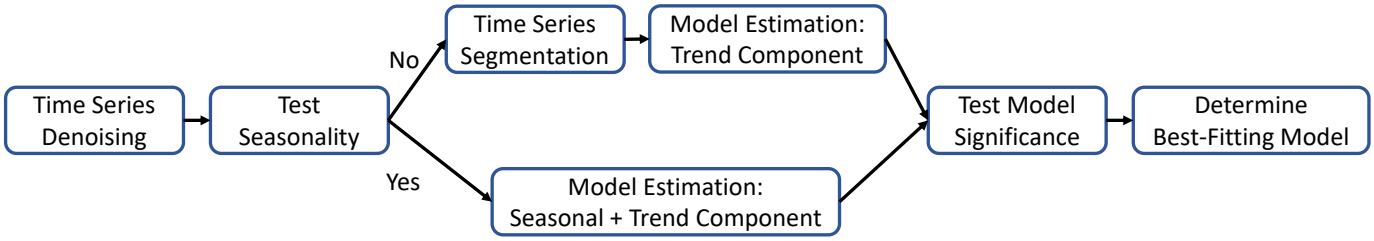

Figure 2. Workflow of PSDefoPAT® [7].

over a wide area. In contrast to InSAR, PSI uses a time series of SAR images to identify pixels with a low noise level to reduce the influence that phase decorrelation and the atmospheric phase delay have on the deformation estimates. The algorithms that implemented this concept were developed by, e.g., Ferretti and Hooper [13, 14]. An adapted version of the StaMPS PSI algorithm, which can be used in a Windows-based framework, was used in this study to process Dataset A.

As stated previously, Dataset B was obtained from the EGMS. Processing the S1 SAR images for the EGMS with advanced DInSAR algorithms was carried out by four different companies, e-GEOS, TRE Altamira, NORCE, and GAF, who each have their own well-established processing chains. DSs were not taken into consideration for all regions processed in the EGMS. The type of scatterer, PS or DS, is indicated by the attribute field "mp_type" in the downloaded EGMS datasets [15]. In the case of the northwestern region of the Peloponnese Peninsula, no MPs marked as DS were identified in the EGMS dataset. The service distributes several InSAR products at different processing levels: (1) Level 2a (L2a), (2) Level 2b (L2b), and (3) Level 3 (L3). The L2a datasets are precise InSAR displacement measurements in the line-of-sight (LOS) of the sensor. The displacements are relative values calculated with a local reference point. The L2b displacements were calibrated with a Global Navigation Satellite System (GNSS) model and are no longer relative measurements. L2b datasets in ascending and descending geometry were used to calculate the horizontal and vertical displacements for the L3 datasets [12]. For this study, we used an L2a dataset.

In addition to an analysis of the spatial deformation pattern, based on mean deformation velocity maps, both datasets were processed with the Fraunhofer IOSB tool PSDefoPAT® [7] to analyze temporal deformation patterns. PSDefoPAT® extracts relevant information on the temporal deformation patterns not directly visible in the typically presented mean deformation velocity maps.

3.2 Persistent Scatterer Deformation Pattern Analysis Tool (PSDefoPAT®)

The tool PSDefoPAT® was developed at Fraunhofer IOSB to ease the analysis of the individual displacement time series of a large set of PS [7]. Most PSI algorithms provide a map of the mean velocity of each PS found in the area of interest and the associated displacement time series for each PS. The advantage of the mean velocity maps is that areas of active deformation are easily recognizable. Also, their spatial expansion and the direction of the deformation in the LOS of the sensors are provided. However, the mean velocity is calculated assuming the deformation is linear. More complex deformation patterns are not considered, such as a periodically varying surface deformation or an accelerating or decelerating deformation pattern. Thus, information on the dynamic nature of the deformation is completely lost to the analyst. PSDefoPAT® estimates the best-fitting model to describe the deformation pattern of each PS over time and thus provides information on the dynamic nature of the deformation. PSDefoPAT® separates the long-term trend, periodic, and noise components of each displacement time series in six steps. The order of these steps is illustrated in Figure 2. The displacement time series is first denoised using wavelet transformation. Afterward, the periodogram of the remaining time series is calculated, and a Fisher's g-test is conducted to determine whether or not the time series has a significant seasonal component. If the time series has such a component, the seasonal and trend components are estimated in one step.

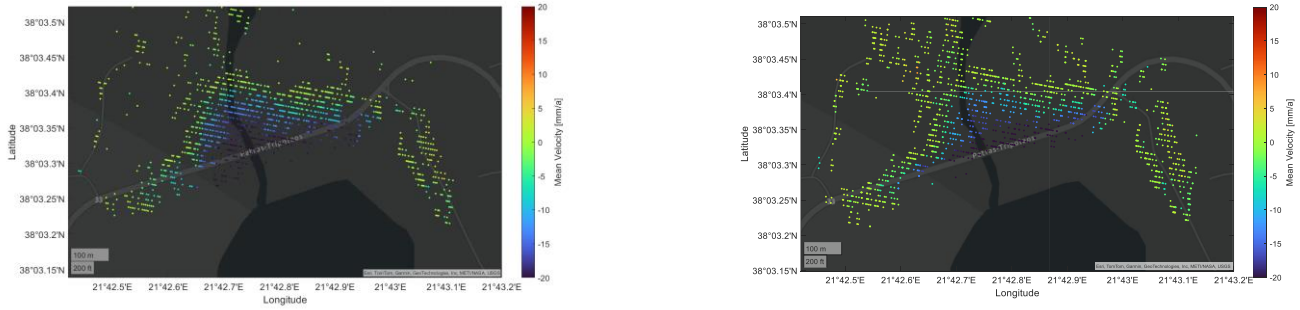

(a) Dataset A (b) Dataset B

Figure 3. Mean deformation velocity for MPs on the dam body of the Parapeiros-Peiros dam in Greece.

DOI: 10.3217/978-3-99161-057-1-165

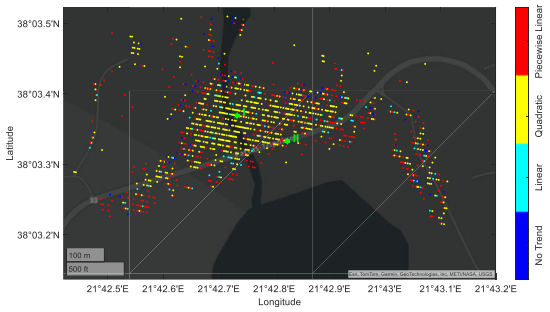

(a) Trend component for Dataset A

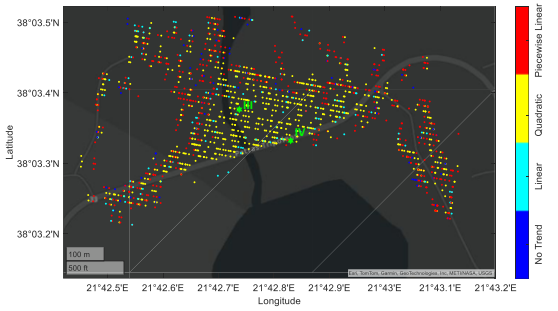

(b) Trend component for Dataset B

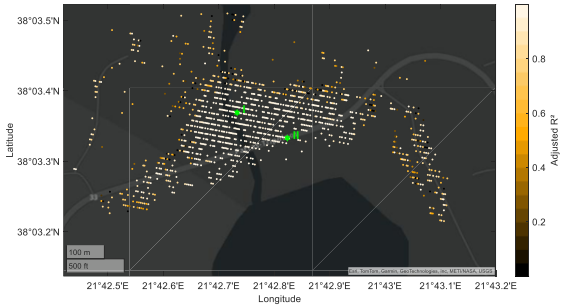

(c) Goodness of the fit for Dataset A

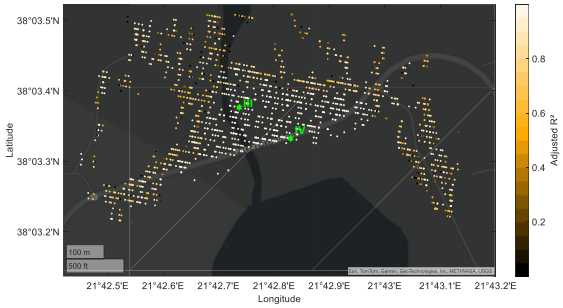

(d) Goodness of the fit for Dataset B

Figure 4. Trend component and the goodness of the fit for the entire time series model.

Valid time series models are (1) purely seasonal, (2) seasonal with a linear trend, and (3) seasonal with a quadratic trend. Only the trend component is estimated if the time series has no significant seasonal component. Applicable models for the trend component are (1) linear, (2) piecewise linear, and (3) quadratic time series models. Before the different models are estimated, the time series is segmented using a top-down segmentation algorithm to provide change points for a piecewise linear model. Lastly, the best-fitting model is determined using the Bayesian Information Criterion (BIC) and the value for the adjusted coefficient of determination R^2_{adj}. Both parameters provide information on the goodness of the fit, taking into consideration the complexity of the model and, therefore, preventing overfitting [7]. PSDefoPAT® automatically generates four plots by default to visualize its results. The plots indicate: (1) the type of trend component, whether or not the time series features a periodic component, (3) the amplitude of the periodic component, and (4) the goodness of fit for the entire time series model. A practical example of these plots is presented in Figure 4 and Figure 5, which visualize the results for the Parapeiros-Peiros dam. With these plots the temporal deformation pattern, not directly visible in the typically presented mean deformation maps, of the MPs in the AOI can be analyzed. For example, MPs effected by a periodic behavior can be easily spotted.

4 RESULTS AND INTERPRETATION

In the following section the results generated with PSDefoPAT® for Dataset A processed by Fraunhofer IOSB and Dataset B obtained from the EGMS are presented and the fit of exemplarily displacement time series and the estimated time series models of individual MPs are discussed.

The mean deformation velocities for the measuring points (MP) in Dataset A and Dataset B located on the dam body of the Parapeiros-Peiros dam are presented in Figure 3. The color map ranges from red, indicating a deformation velocity larger than 20 mm/y in the direction towards the sensor, to blue, indicating a deformation velocity larger than -20 mm/y in the direction away from the sensor. Both images show that the mean deformation velocity on the dam body varies along the downstream shoulder, with more -20 mm/y at the crown and close to zero at the toe of the dam body. This is a typical spatial deformation pattern observed for embankment dams [16]. In order to analyze the temporal deformation pattern, the displacement time series of Dataset A and Dataset B were processed with PSDefoPAT®. The results are visualized in Figure 4 and Figure 5. Figure 4 (a) showing Dataset A and (b) Dataset B indicate whether the processed displacement time series exhibit a linear (cyan), quadratic (yellow), piecewise linear (red) trend, or no trend (blue). In both cases, the majority of MPs at the center of the downstream shoulder of the dam body exhibit a quadratic trend, and MPs located closer to the edges or adjacent to the dam exhibit a piecewise linear trend. This pattern is mirrored in Figure 4 (c) and Figure 4 (d), which present a measure for the goodness-of-fit in the form of the adjusted coefficient of determination R^2_{adj} for the estimated time series model for Dataset A and B, respectively. The estimated time series model for MPs at the center of the dam body fit the displacement time series better than those estimated for MPs at the edge of the dam body, for both Datasets.

DOI: 10.3217/978-3-99161-057-1-165

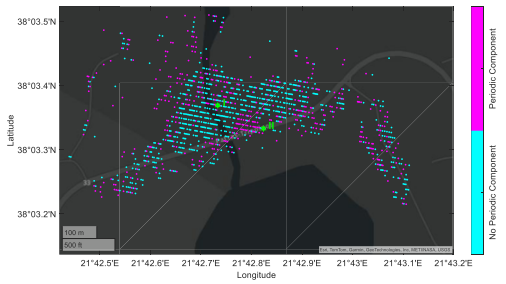

(a) Indication of a periodic component for Dataset A

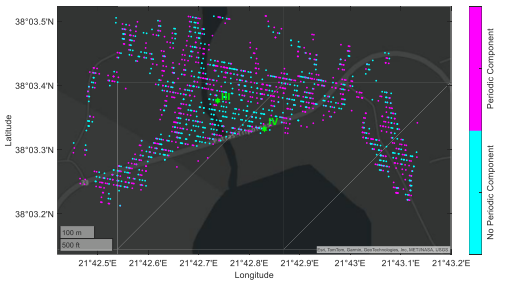

(b) Indication of a periodic component for Dataset B

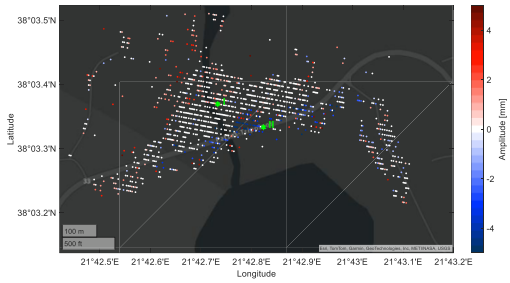

(c) Amplitude of the periodic component for Dataset A

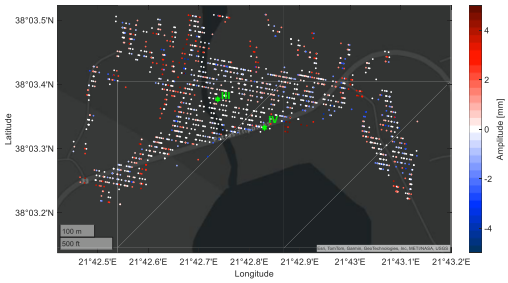

(d) Amplitude of the periodic component for Dataset B

Figure 5. Periodic component and the corresponding amplitude of the periodic component.

Figure 5 indicates whether the estimated time series model includes a periodic component (magenta) or not (cyan), along with the corresponding amplitude of the periodic component. While the estimated time series models for Dataset A, see Figure 5 (a) and Figure 5 (c), show that only some MPs exhibit a periodic behavior, in the case of Dataset B, see Figure 5 (b) and Figure 5 (d), significantly more MPs exhibit periodic behavior. This may be due to the different time spans that Dataset A and Dataset B cover. In order to investigate the displacement time series and estimated time series models further, we examined four exemplary MPs located at the downstream shoulder (MP I and MP III) and crown (MP II and MP IV) of the dam body for both datasets. The MPs are marked in green in Figure 4 and Figure 5. The selected MPs for both datasets are not identical, however, they were picked as closely together as possible to ensure comparability. Their displacement time series (black dots), overall estimated time series model (green), and the lower and upper error margins (red) are presented in Figure 6 and Figure 7. The estimated parameters for the time series models are also summarized in Table 1. Figure 6 displays the displacement time series for MP I and MP III, which are located on the downstream shoulder of the dam body. Both estimated time series models exhibit a quadratic trend. While the linear coefficients of both models are similar, with $-11.1\,\mathrm{mm/y}$ for MP I and $-10.1\,\mathrm{mm/y}$ for MP III, the scaling parameter of quadratic time series model differs. The scaling parameter is estimated to be $-1\,\mathrm{mm^2/y^2}$ for MP I and $-0.5\,\mathrm{mm^2/y^2}$ for MP III. A smaller value for the scaling parameter leads to a wider opening for the parabola, approximating the displacement time series. This difference in the scaling parameter might be influenced by the slightly different time spans that Dataset A and Dataset B cover. While Dataset A covers only the time of the first filling of the freshwater reservoir, Dataset B covers a short time before the first filling and about a year afterwards.

Table 1. Model parameters and estimated mean velocity of the selected MPs.

	Mean Velocity	Best-Fitting Model	R^2_{adj}
Downstream Crown:			
Dataset A	$-25.1\,\mathrm{mm/a}$	$d = -29.7\ \mathrm{mm/a} \cdot t + 2\,\mathrm{mm^2/a^2} \cdot t^2 - 4.6 \cdot \sin(\frac{2\pi}{798.3\mathrm{d}}(t - 391.9\ \mathrm{d}))$	0.99
Dataset B	$-28.1\,\mathrm{mm/a}$	$d = -26.6\ \mathrm{mm/a} \cdot t - 0.3\,\mathrm{mm^2/a^2} \cdot t^2 - 1.6 \cdot \sin(\frac{2\pi}{519.9d}(t - 119.4\ \mathrm{d}))$	0.99
Downstream Shoulder:			
Dataset A	$-16.1\,\mathrm{mm/a}$	$d = -11.14\ \mathrm{mm/a} \cdot t - 1.0 \cdot t^2\ \mathrm{mm^2/a^2}$	0.99
Dataset B	$-17\ \mathrm{mm/a}$	$d = -10.1\ \mathrm{mm/a} \cdot t - 0.5\,\mathrm{mm^2/a^2} \cdot t^2$	0.99

DOI: 10.3217/978-3-99161-057-1-165

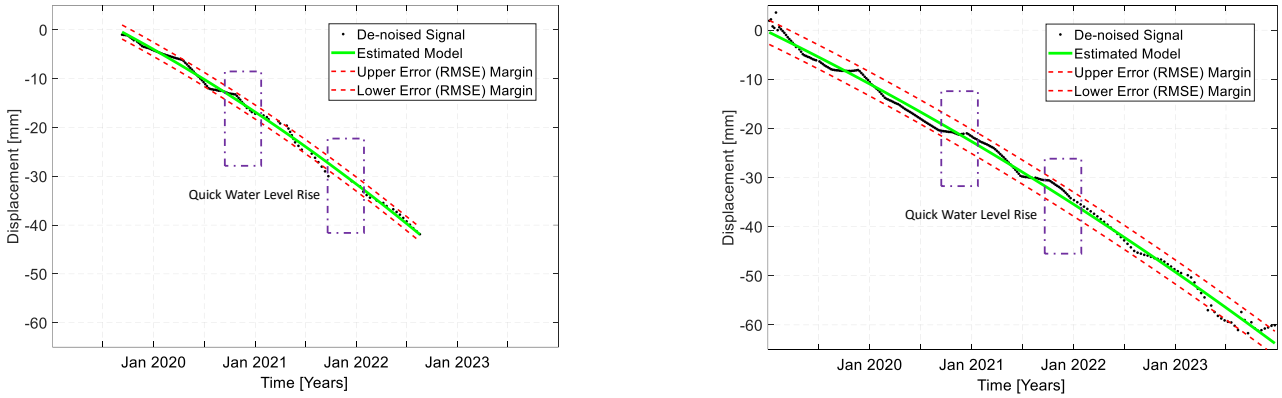

(a) MP I in Dataset A (b) MP III in Dataset B

Figure 6. The displacement time series (black dots), overall estimated time series model (green), and the lower and upper error margins (red) for MP I and MP III, which are located on the downstream shoulder of the Parapeiros-Peiros dam.

The estimated time series model of MP II and MP IV, which are located on the downstream side of the crown, are presented in Figure 7. Again, both displacement time series are approximated by a quadratic model for the trend component. The values of the linear coefficient are significantly higher than those estimated for MP I and MP III. The coefficients were estimated to be $-29.7\,\mathrm{mm/y}$ for MP II and $-28.1\,\mathrm{mm/y}$ for MP IV. The observed varying deformation rates from the crown of the dam body, along its shoulder to the toe, are common for embankment dams [16]. Additionally, both time series models have a periodic component. However, the estimated amplitude and cycle length of the periodic component for MP II and MP IV diverge from one another. The amplitude is -4.6 mm for MP II and -1.6 mm for MP IV, and the corresponding cycle lengths are 798.3 d and 519.9 d, respectively. These differences are again possibly influenced by the varying time span the datasets cover. Two events of quick water level rise in the reservoir occurred during the filling process [17]. The first one occurred in late 2020 and the second one in late 2021, both time spans are marked in purple in Figure 6 and Figure 7. The displacement time series of MP II diverges significantly from the quadratic during this time, see Figure 6 (a). The displacement time series of MP IV also diverges from its trend during this time, see Figure 7 (b). However, the periodic component is not as prominent as in the time series model of MP II. This might be due to the more extended time span that the displacement time series of MP IV covers. The displacement time series includes data from 2022 and 2023, in addition to 2020 and 2021. The events of accelerated water level rise from fall and winter 2020 and 2021 did not repeat in the same severity at the end of 2022 and 2023. Therefore, the displacements due to these events have been smoothed over in the longer displacement time series and thus have led to different estimations for the periodic component of MP IV in comparison to MP II.

Based on the analysis of the mean deformation velocity maps, presented in Figure 3, the spatial deformation pattern of both datasets for the Parapeiros-Peiros dam are very similar. Using PSDefoPAT® in post-processing to analyze the temporal deformation pattern reveals that short-term temporal deformation patterns are not only smoothed over in the mean deformation map but also in cases where longer time series, such as Dataset B, are used. Highlighting the advantage of customizing the dataset to a specific time span that needs to be examined. For infrastructure monitoring, both long-term trends and short-term events are of interest. Thus, in-house processing of SAR images for surface deformation monitoring is still necessary.

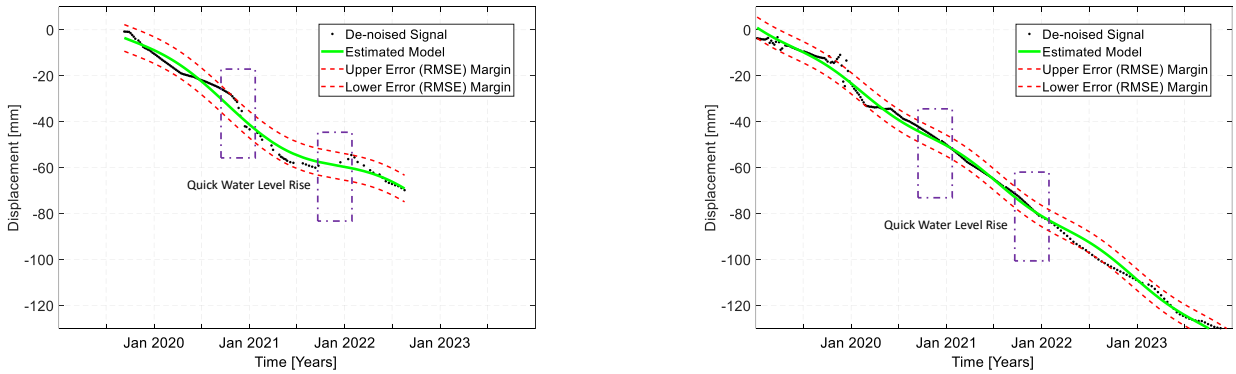

(a) MP II in Dataset A (b) MP IV in Dataset B

Figure 7. The displacement time series (black dots), the overall estimated time series model (red), and the lower and upper error margins (red) for MP II and MP IV, which are located on the downstream crown of the Parapeiros-Peiros dam.

DOI: 10.3217/978-3-99161-057-1-165

5 SUMMARY

In this study, we examined the surface deformation of the Parapeiros-Peiros dam during its first filling and shortly after, based on two datasets. The first dataset consists of 119 S1 SAR images and was processed in-house. The second dataset was downloaded from the EGMS. The observable spatial and temporal deformation patterns of both datasets were compared to explore the necessity for in-house advanced DInSAR processing for surface deformation monitoring of critical infrastructure, such as a newly built dam. An analysis of the spatial deformation patterns based on the mean deformation velocity maps showed good agreement between both datasets and that the highest deformation rates can be observed at the crown of the dam body, which agrees with the spatial deformation pattern typically observed in embankment dams [15]. The analysis of observable temporal deformation patterns, not directly visible in the mean velocity maps, was aided by the post-processing tool PSDefoPAT® developed by Fraunhofer IOSB. The tool extracts relevant information on the temporal deformation pattern of advanced DInSAR datasets by automatically determining the best-fitting time series model for each displacement time series of the dataset. In the case of the two datasets examined in this study, it was revealed that short-term displacement events are not only smoothed out in the mean deformation velocity maps but also in cases where longer time series are examined, e.g., Dataset B. Both long-term displacement trends and short-term events of diverging displacements are important to document and analyze in infrastructure monitoring. Pointing out a disadvantage of using the EGMS for infrastructure monitoring, which always examines a time span of five years. Another disadvantage is the time delay in providing the data, which is currently at a minimum of three-quarters of a year. Both of these aspects led us to the conclusion that the possibility of customizing the dataset to the deformation phenomena in question and the timelier fashion of processing still render in-house processing of SAR images for surface deformation monitoring of infrastructure necessary.

REFERENCES

[1] Scaioni, M., Marsella, M., Crosetto, M., Tornatore, V., Wang, J. “Geodetic and remote-sensing sensors for dam deformation monitoring”, Sensors, vol. 18, no. 11, p. 25, 2018.
[2] ICOLD, CIGB. “Automated dam monitoring systems: guidelines and case histories”, International Commission on Large Dams, vol. 151, 2000.
[3] Icold-cigb.org. “International Commission on Large Dams”, (2022), https://icold-cigb.org/ (22.12.2022).
[4] Hunter, G., Fell, R., “The deformation behaviour of embankment dams”, University of New South Wales, School of Civil and Environmental Engineering, 2003.
[5] Sousa, J. J., Bastos, L., “Multi-temporal SAR interferometry reveals acceleration of bridge sinking before collapse”, Natural Hazards & Earth System Sciences, vol. 13, no. 3, pp. 659-659, 2013.
[6] Tomás, R., Cano, M., Garcia-Barba, J., Vicente, F., Herrera, G., Lopez-Sanchez, J. M., Mallorquí, J. J., “Monitoring an earthfill dam using differential SAR interferometry: La Pedrera dam, Alicante, Spain”, Engineering Geology, vol. 157, pp. 21-32, 2013.
[7] Evers, M., Thiele, A., Hammer, H., & Hinz, S. (2023). PSDefoPAT—persistent scatterer deformation pattern analysis tool. Remote Sensing, vol. 15, no. 19, 4646.
[8] Demetrakopoulos, A. K., Dimas, A. A., Kaleris, B. K, Yannopoulos, P. X., Manariotis, I. D., Chasiakos, A., Podimata M., Lepidas, F., “Dam operator of the water project ‘Water supply of Patras city, Patras Industrial Zone and Northwest settlements of Achaia prefecture via the Peiros and Parapeiros Rivers’”, University of Patras, Patras, pp. 1-136, 2013 (in Greek).
[9] Podimata, M. V., Yannopoulos, P. C., “A road map for resolving conflicts in dam’s administration: The case of Peiros - Parapeiros dam in Greece”, European Water, vol. 60, pp. 415-421, 2017.
[10] Evers, M., Kyriou, A., Thiele, A., Hammer, H., Nikolakopoulos, K., Schulz, K., “How to set up a dam monitoring system with PSInSAR and GPS”, Proc. SPIE 11534, Earth Resources and Environmental Remote Sensing/GIS Applications XI, vol. 11534, pp. 98-114, 2020.
[11] Corns, C. F., “Gravity Dam Design and Analysis”, in Jansen, R. B. (ed.) Advanced dam engineering for design, construction, and rehabilitation. Springer Science & Business Media, pp. 466-492, 2012.
[12] Costantini, M., Minati, F., Trillo, F., Ferretti, A., Novali, F., Passera, E., Andersen, H., “European Ground Motion Service (EGMS)”, 2021 IEEE International Geoscience and Remote Sensing Symposium IGARSS, pp. 3293-3296, 2021.
[13] Ferretti, A., Prati, C., Rocca, F., “Permanent scatterers in SAR interferometry”, IEEE Transactions on Geoscience and Remote Sensing, vol. 39, no. 1, pp. 8-20, 2001.
[14] Hooper, A., Zebker, H., Segall, P., Kampes, B. “A new method for measuring deformation on volcanoes and other natural terrains using InSAR persistent scatterers”, Geophysical Research Letters, vol. 31, no. 23, L23611, 2004.
[15] Capes, R., Passera, E.,” End-to-end implementation and operation of the European Ground Motion Service (EGMS)”, vol. 2, p. 33, 2023, https://land.copernicus.eu/en/technical-library/egms-product-description-document/@@download/file
[16] Kutzner, C. (2018). Earth and rockfill dams: Principles for design and construction.
[17] Dounias, G.; Lazaridou, S.; Sakellariou, S.; Somakos, L.; Skourlis, K.; Mihas, S. The behavior of Asteri Dam on Parapeiros River during first filling, Greece. In Proceedings of the 91st International Commission of Large Dams Annual Meeting, International Commission of Large Dams, Gothenburg, Sweden, 20 June 2023; pp. 1–10.